An efficient static solver for the lattice discrete particle model (LDPM)

Presenter: Alessandro Fascetti

Authors: Dongge Jia[1], John C. Brigham[1,2] Alessandro Fascetti[1]
[1] Department of Civil and Environmental Engineering, University of Pittsburgh
[2] Department of Bioengineering, University of Pittsburgh

Background and Motivation

- In the last decade, the lattice discrete particle model (LDPM) has become one of the most appealing computational tools to simulate fracture in quasi-brittle materials such as concrete, shale, masonry, high-performance cementitious composites, rocks, and polymers.
- All LDPM-based modelling relied on the sole solution strategy: dynamic explicit algorithm with a central difference scheme.
- Drawbacks of explicit dynamic solutions for quasi-static condition:
  1. Conditional stability in elastic stage, and consequent computational demanding;
  2. Undermined accuracy when simulating locally instable issue (quasi-brittle fracture).

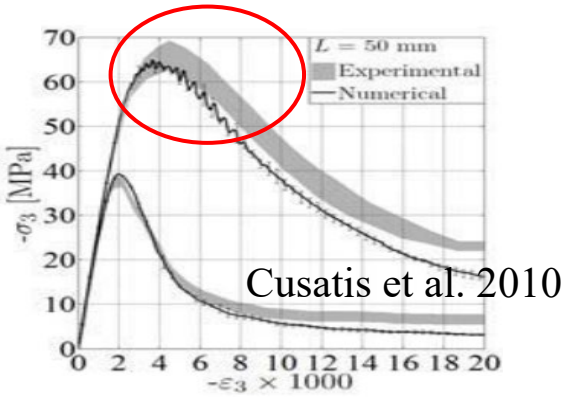

Cusatis et al. 2010

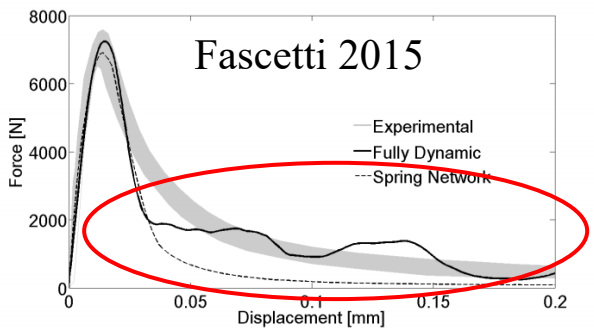

Figure 5.28: Notched specimen: fully dynamic vs spring network models

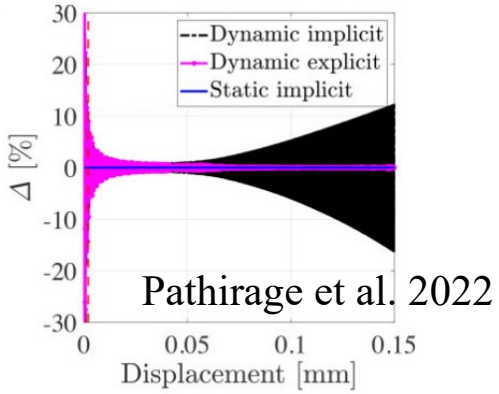

Pathirage et al. 2022

Objective and Innovation

The goal is to

(1) Develop a static solver capable of solving LDPM;

(2) Compare the computational efficiency between static solution and dynamic solution;

(3) Enable the evaluation of the performance of dynamic solution against the equilibrium path captured by static solution.

An efficient static solver is realized by

(1) Modification of the LDPM constitutive law to render the material response continuity;

(2) Arc-length method with adaptive criterion to select the sign of the initial load increment factor;

(3) Adaptive path switch mechanism to restrict oscillations in the global stiffness matrix caused by LDPM unloading-reloading rules;

(4) Computationally efficient implementation with automatic differentiation aided by graph coloring.

Lattice discrete particle model (LDPM)

Realistic geometrical representation of heterogeneous material (concrete)

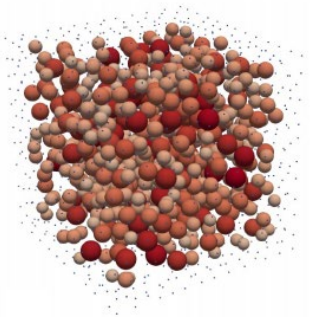

Aggregate distribution

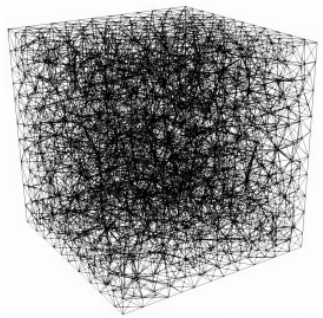

Delauney tetrahedralization

LDPM tessellation

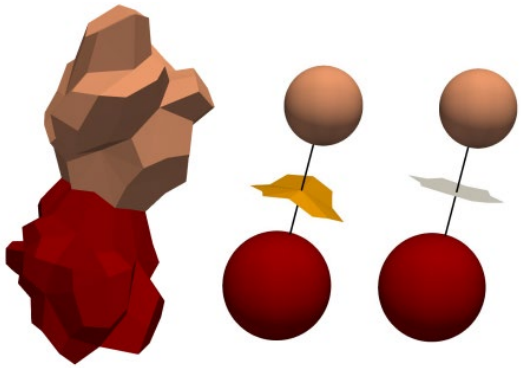

Two aggregates sharing (projected) contact areas

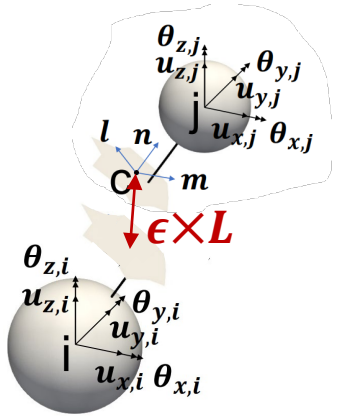

Nodal degrees of freedom and facet strain of a lattice element

Discrete strain compatibility and force equilibrium equations

A displacement jump is transformed into facet strains by dividing by the lattice element length:

$$\epsilon_{Nk} = \mathbf{n}_k^T [\![\mathbf{u}_{Ck}]\!]/l_e = \mathbf{B}_N^{jk}\mathbf{Q}_j - \mathbf{B}_N^{ik}\mathbf{Q}_i$$

$$\epsilon_{Lk} = \mathbf{l}_k^T [\![\mathbf{u}_{Ck}]\!]/l_e = \mathbf{B}_L^{jk}\mathbf{Q}_j - \mathbf{B}_L^{ik}\mathbf{Q}_i$$

$$\epsilon_{Mk} = \mathbf{m}_k^T [\![\mathbf{u}_{Ck}]\!]/l_e = \mathbf{B}_M^{jk}\mathbf{Q}_j - \mathbf{B}_M^{ik}\mathbf{Q}_i$$

The nodal forces at nodes i and j associated with facet k are obtained:

$$\mathbf{F}_{ik}^T = -l_e A_k(\sigma_{Nk}\mathbf{B}_N^{ik} + \sigma_{Mk}\mathbf{B}_M^{ik} + \sigma_{Lk}\mathbf{B}_L^{ik})$$

$$\mathbf{F}_{jk}^T = l_e A_k(\sigma_{Nk}\mathbf{B}_N^{kj} + \sigma_{Mk}\mathbf{B}_M^{kj} + \sigma_{Lk}\mathbf{B}_L^{kj})$$

Summing up the nodal forces at all nodes and equating it to the external force provides the LDPM equilibrium equations.

Lattice discrete particle model (LDPM)

Normal-tangential coupled lattice-level stress-strain constitutive with material response continuity

On each lattice element, given effective stress $\sigma = \sqrt{\sigma_N^2 + \frac{\sigma_T^2}{\alpha}}$ and effective strain $\epsilon = \sqrt{\epsilon_N^2 + \alpha\epsilon_T^2}$, and $\omega = \arctan\frac{\epsilon_N}{\sqrt{\alpha}\epsilon_T}$, the constitutive las is

Effective stress vs. effective strain under different stress states

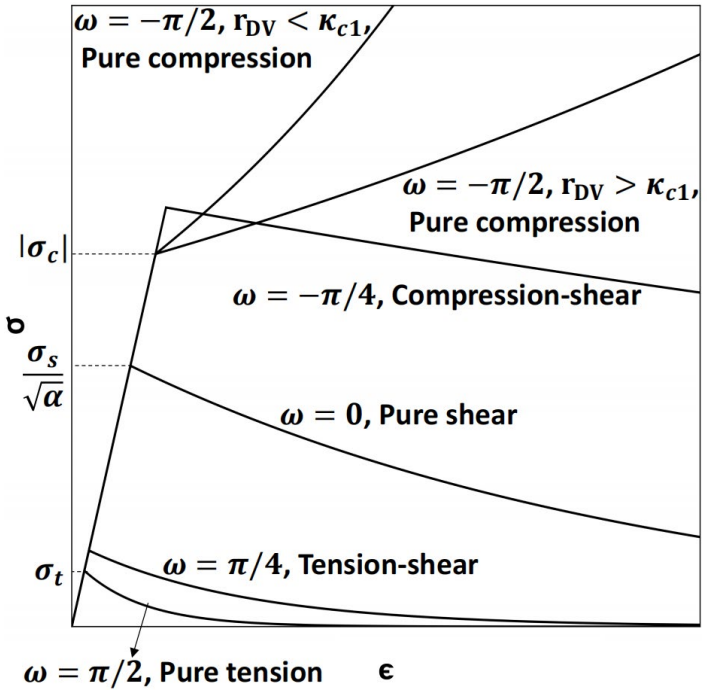

The boundary for elastic stage is

$$\sigma(\omega) = \frac{sin\omega(\sigma_c + \sigma_t) + \sqrt{D}}{2(sin^2\omega - cos^2\omega\alpha\sigma_c\sigma_t/\sigma_s^2)}$$

where

$$D = sin^2\omega(\sigma_c + \sigma_t)^2 - 4\sigma_c\sigma_t(sin^2\omega - cos^2\omega\alpha\sigma_c\sigma_t/\sigma_s^2)$$

If visualized in terms of normal and tangential stress:

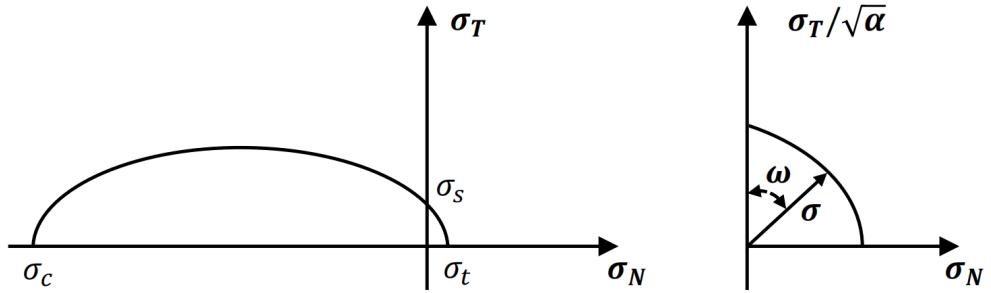

An adaptive arc-length method

First-order approximation to static force equilibrium

$$\begin{aligned}\mathbf{R}(\mathbf{u}', \lambda') &= \mathbf{R}(\mathbf{u_0}, \lambda_0) + (\frac{\partial \mathbf{R}}{\partial \lambda})\delta\lambda + (\frac{\partial \mathbf{R}}{\partial \mathbf{u}})\delta\mathbf{u} \\ &= \mathbf{R}(\mathbf{u_0}, \lambda_0) + -\mathbf{q}\delta\lambda + \mathbf{K}_T\delta\mathbf{u} \\ &= \mathbf{0}\end{aligned}$$

Iterate both force and displacement

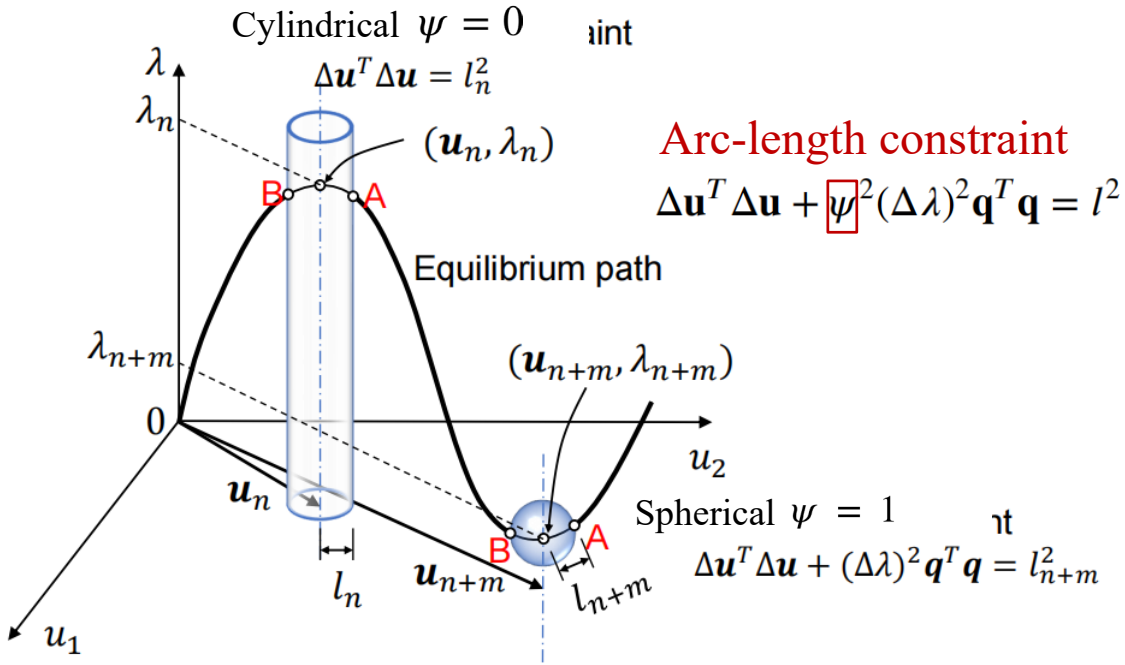

Arc-length constraint

$$\Delta\mathbf{u}^T\Delta\mathbf{u} + \psi^2(\Delta\lambda)^2\mathbf{q}^T\mathbf{q} = l^2$$

The proposed collaborative criterion to determine the sign of the initial increments of the load factor

$$\mathbf{F}^{ext} = \lambda\mathbf{q}$$

$$\delta\bar{\mathbf{u}} \equiv \mathbf{K}_T^{-1}\mathbf{q}$$

#1 $$\text{sign}(\delta\lambda_{k,1}) = \begin{cases} \text{sign}(\text{mean}(\delta\bar{\mathbf{u}}^l)) & \text{if } \mathbf{q}^l > \mathbf{0} \\ -\text{sign}(\text{mean}(\delta\bar{\mathbf{u}}^l)) & \text{if } \mathbf{q}^l < \mathbf{0} \end{cases}$$

#2 $$\text{sign}(\delta\lambda_{k,1}) = \text{sign}(\delta\lambda_{k-1})$$

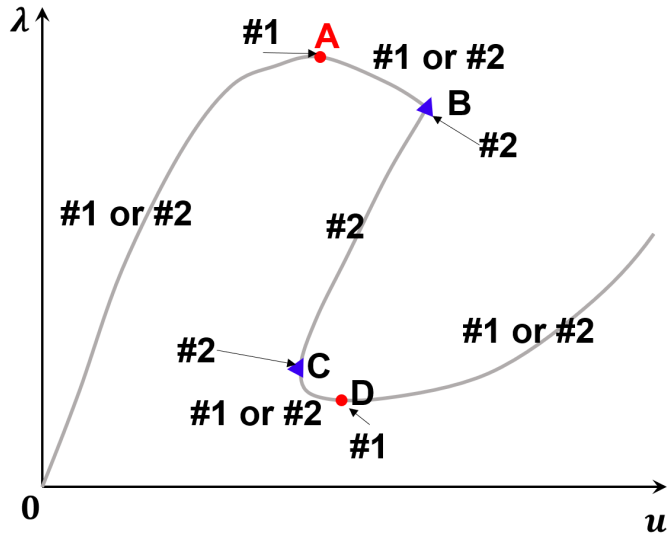

An adaptive arc-length method

For a more continuous Jacobian in $\mathbf{R}(\mathbf{u}_0, \lambda_0) + -\mathbf{q}\delta\lambda + \mathbf{K}_T\delta\mathbf{u} = \mathbf{0}$

A trigonometric parametric transition curve bridging the unloading-reloading path and the strain-softening branch:

$$\sigma = \begin{cases} \sigma_{\text{u-r}}(\epsilon)\left(\frac{1-\sin\left(\frac{\epsilon-\epsilon_{\text{start}}}{\epsilon_{\text{int}}-\epsilon_{\text{start}}}\pi-\frac{\pi}{2}\right)}{2}\right) + (\sigma_{\text{int}} + E_{\text{int}}(\epsilon-\epsilon_{\text{int}}))\frac{1+\sin\left(\frac{\epsilon-\epsilon_{\text{start}}}{\epsilon_{\text{int}}-\epsilon_{\text{start}}}\pi-\frac{\pi}{2}\right)}{2} & \text{if } \epsilon \le \epsilon_{\text{int}} \\ \sigma_{\text{int}} + E_{\text{int}}(\epsilon-\epsilon_{\text{int}}) & \text{if } \epsilon > \epsilon_{\text{int}} \end{cases}$$

Adaptive path switch:

After the completion of each increment, elements are checked to determine whether their constitutive paths are transitioning between limit paths and unloading-reloading paths, and the stress-strain paths will be switched accordingly

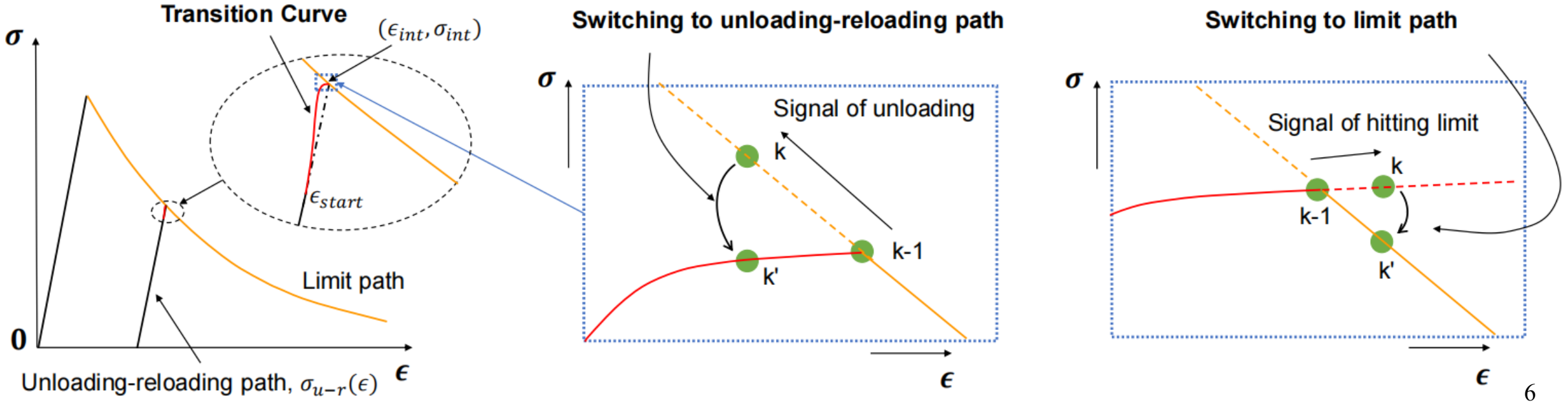

Computationally efficient implementation

Automatic differentiation (AD) with distance-1 graph coloring

$$\frac{\partial \boldsymbol{y}}{\partial x_j} = \frac{\partial \boldsymbol{\eta}_{,v}}{\partial \boldsymbol{\eta}_{,v-1}} \cdots \frac{\partial \boldsymbol{\eta}_{,3}}{\partial \boldsymbol{\eta}_{,2}} \frac{\partial \boldsymbol{\eta}_{,2}}{\partial x_j} \quad \text{(forward mode AD)}$$

The number of required AD passes can be decreased by aggregating multiple independent passes together to allow for the computation of compressed fuller columns (or rows) (Gebremedhin et al. 2005).

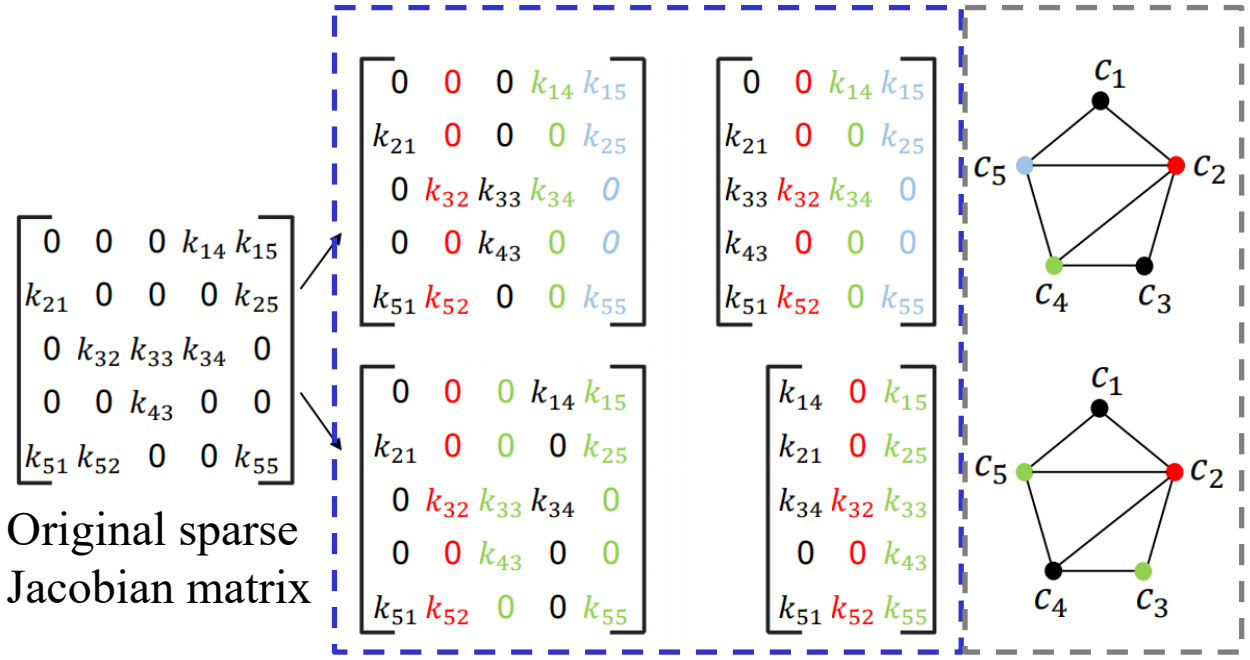

To find the coloring scheme that produces the lowest possible number of compressed columns:

Greedy algorithm: assign each vertice to a sequence number of color that has already been used as much as possible (Curtis et al. 1974).

Largest-first (LF) ordering: organize the vertices in a manner in which the degree of each vertex — representing the number of edges connected to the vertex — is arranged from the largest to the smallest (Welsh and Powell 1967).

Numerical Results

Concrete experiments used for validation and evaluation:

1. Unconfined compression

(Fascetti et al. 2016)

2. Biaxial fracture

(Kupfer et al. 1969)

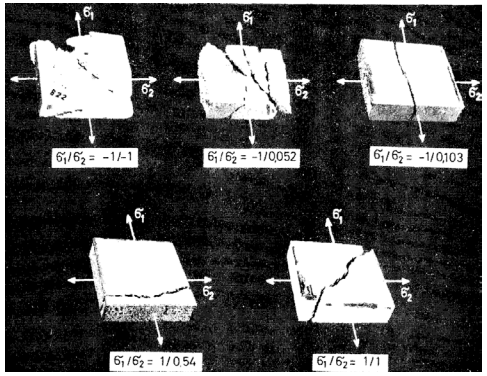

3. Tensile splitting

(Bazant et al. 1991)

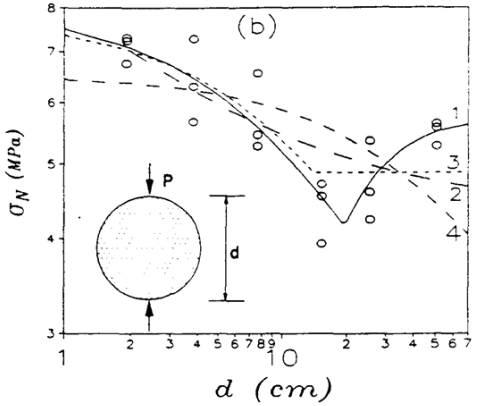

4. 3-point bending

(George et al. 2013)

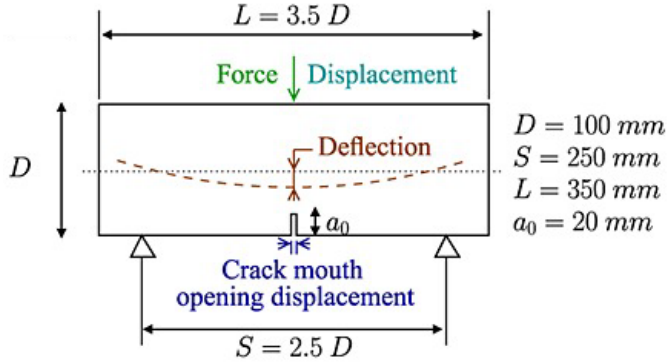

Numerical Results - Parameter Calibration

Parameter calibration

Geometry parameters:

1. Use those already published in the literature.

Mechanical parameters:

1. Choose the values of parameters that already being calibrated in literature;
2. Calibrate a few parameters that have new definition if necessary.

Values of constitutive parameters used in the numerical simulations

Symbol (units)	Unconfined compres-sion	Biaxial behavior	Tensile splitting	three-point flexure
E_0 (MPa)	44000	46260	55610	57180
α (-)	0.21	0.25	0.25	0.25
σ_t (MPa)	3.5	2.89*	4.65	2.62*
G_t (N/mm)	0.04	0.001	0.0194	0.0272*
n_t (-)	1	0.2	0.1	0.2
σ_s/σ_t (-)	10	5.75	2.75	3.276
G_s (N/mm)	0.7	0.7	0.7	0.7
σ_{c0} (MPa)	52	32.6*	150	120
H_{c0}/E_0 (-)	0.056*	0.1	0.4	0.4
κ_{c1} (-)	1	1	1	1
κ_{c2} (-)	5	5	5	5
n_c (-)	2.2*	0.7*	1	1

Note: superscript * indicates calibrated values

Numerical Results - Validation

Cubic sample

Parameter calibration

Cylindrical sample

Validation

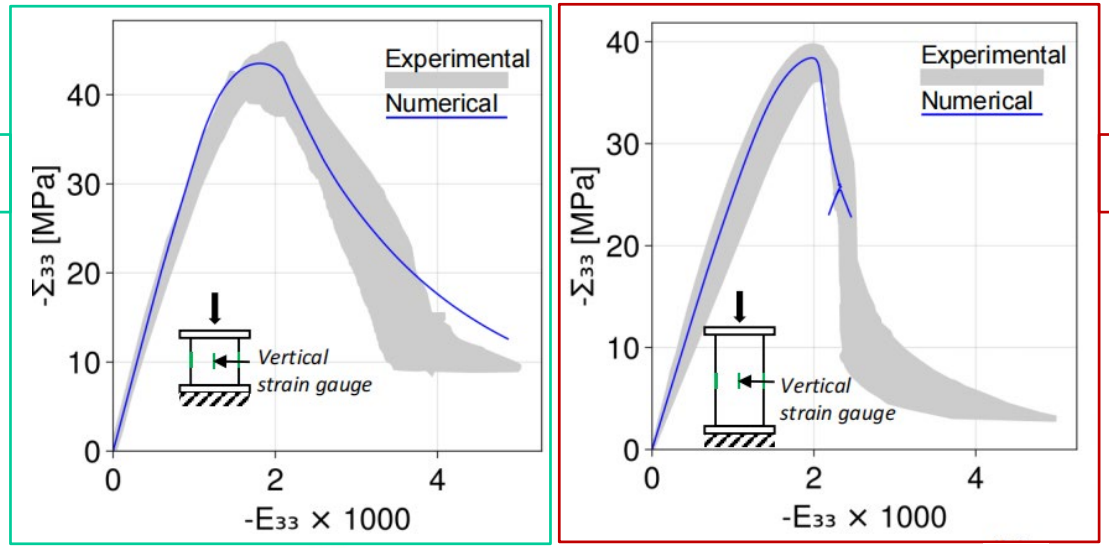

Unconfined Compression

Tested data are from Fascetti et al. (2016)

Stress-strain response

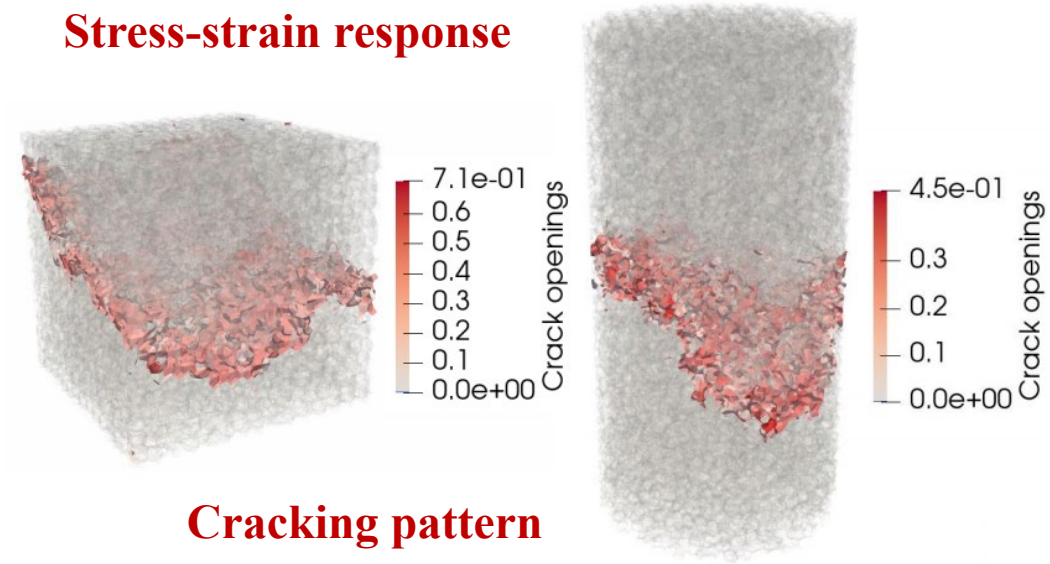

Cracking pattern

Numerical Results - Validation

Biaxial behavior – stress-strain response Tested data are from Kupfer et al. (1969)

Parameter calibration

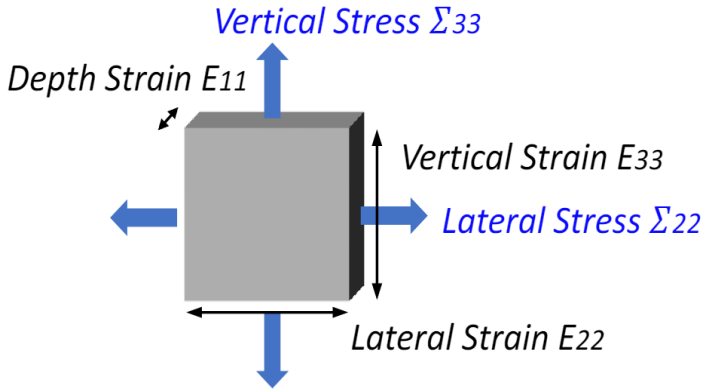

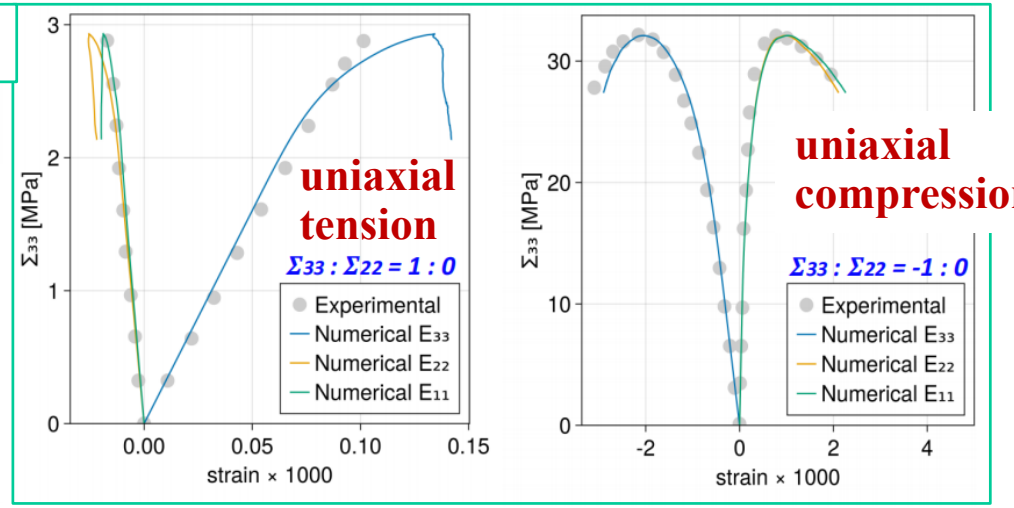

Validation

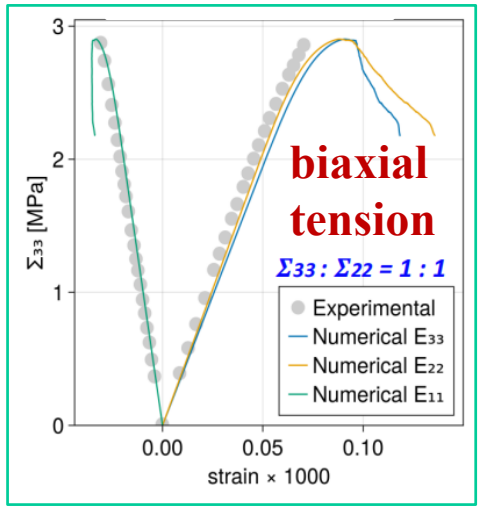

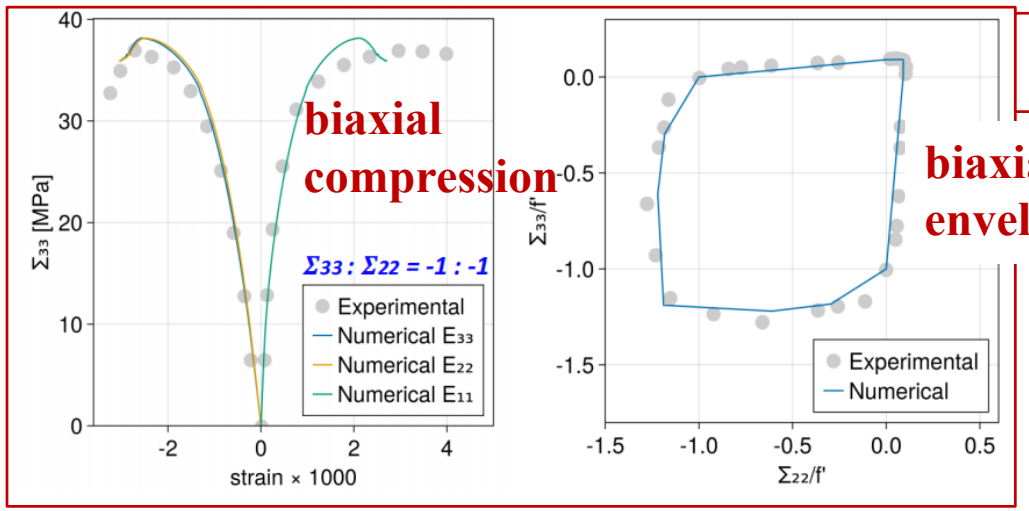

Numerical Results - Validation

Biaxial behavior – cracking pattern

uniaxial tension

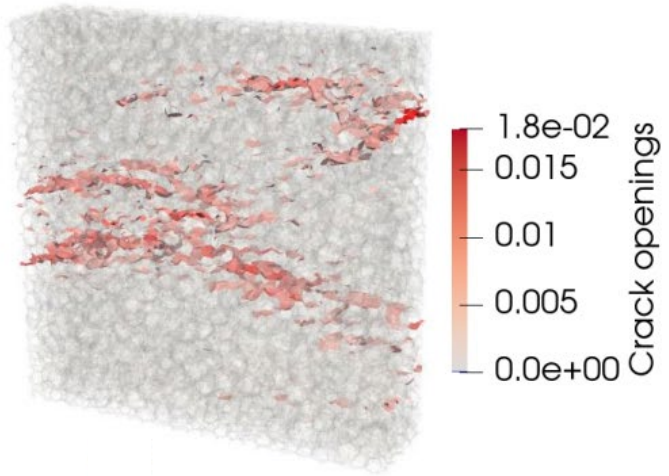

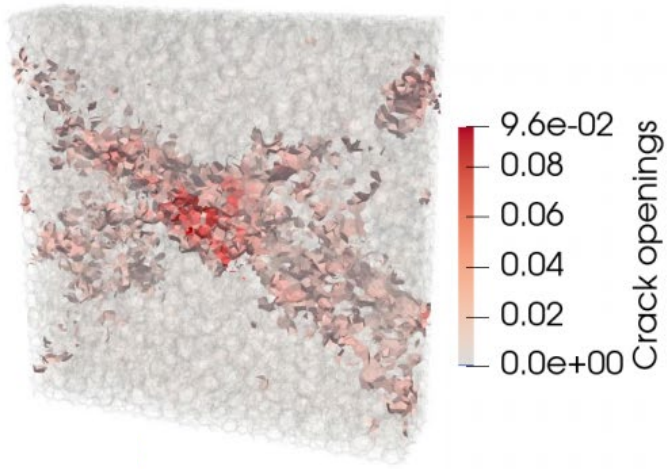

uniaxial compression

biaxial tension

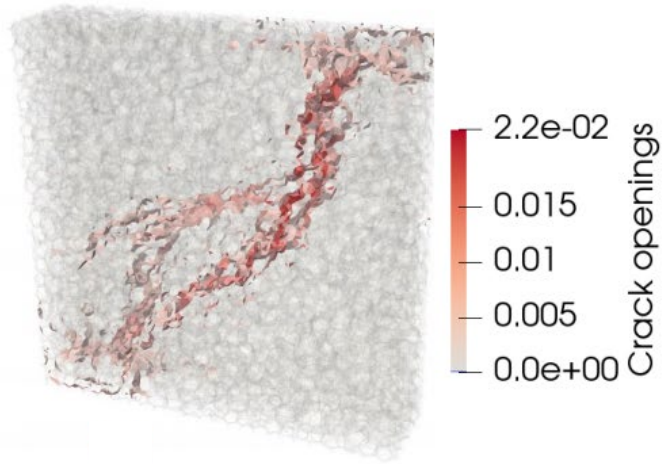

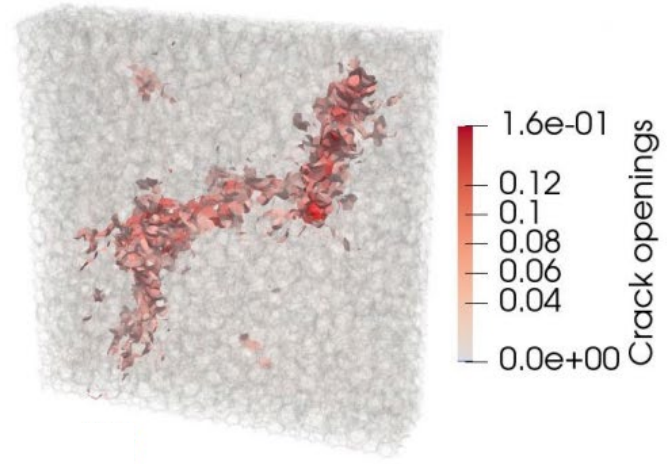

biaxial compression

Numerical Results - Validation

Tensile splitting tests Tested data are from Bazant et al. (1991)

Validation

Parameters are adopted from those calibrated by Cusatis et al. (2011b)

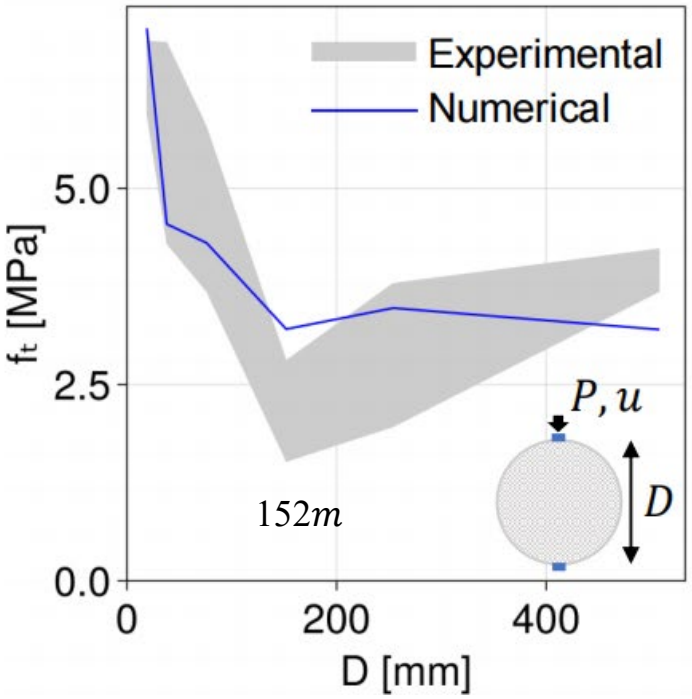

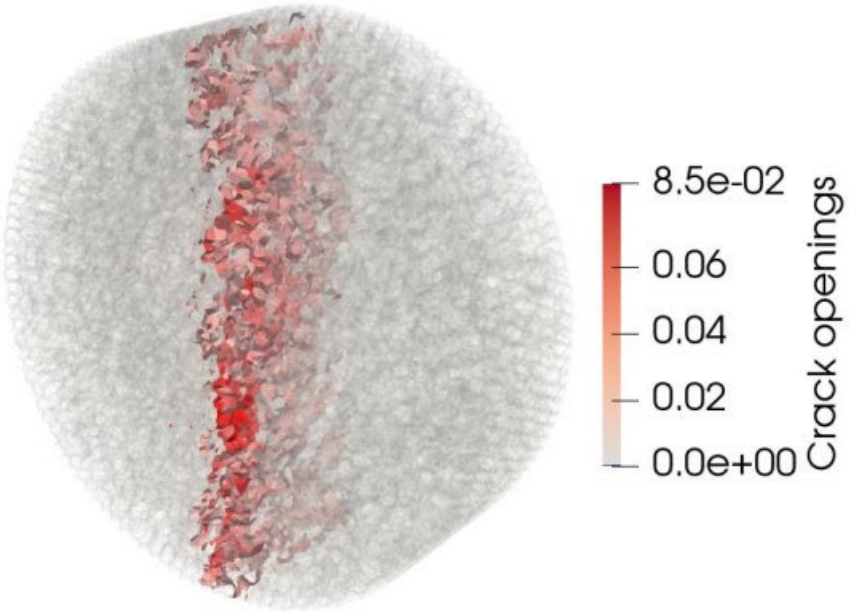

Splitting strength w.r.t. diameter **Cracking pattern**

Numerical Results - Validation

Three-point bending tests

Tested data are from George et al. (2013)

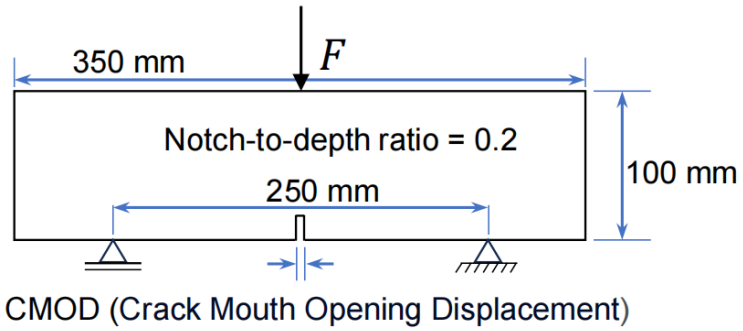

CMOD (Crack Mouth Opening Displacement)

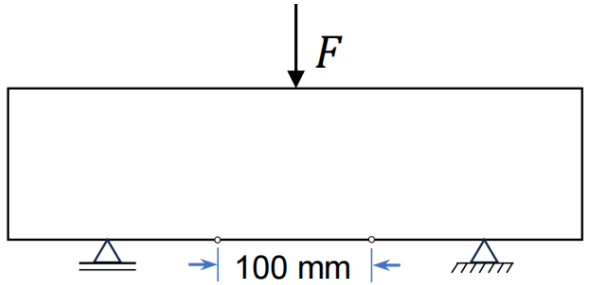

Pseudo CMOD

Parameter calibration

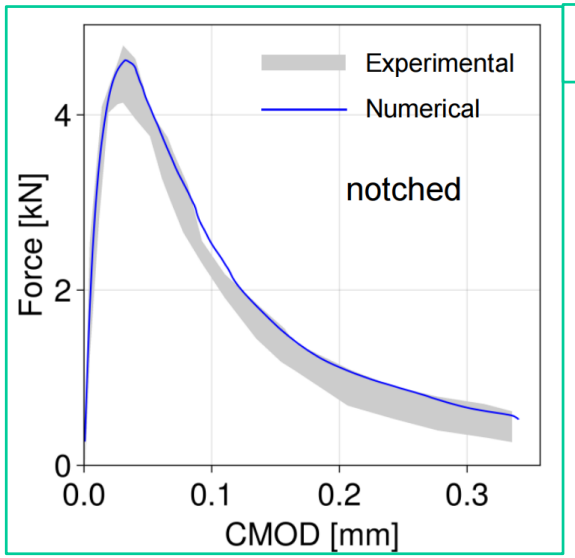

Validation

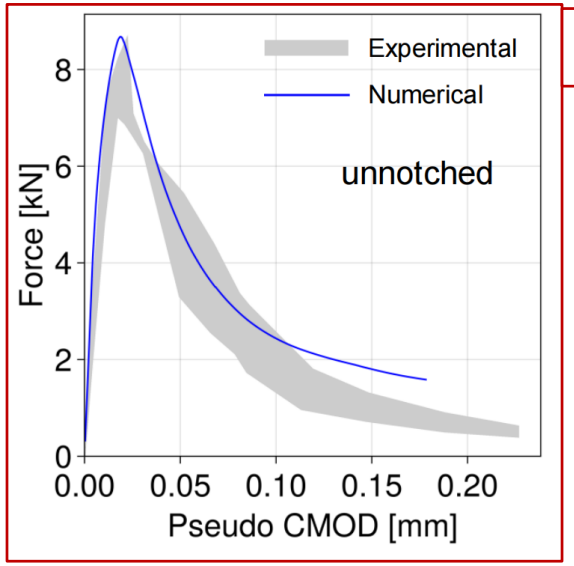

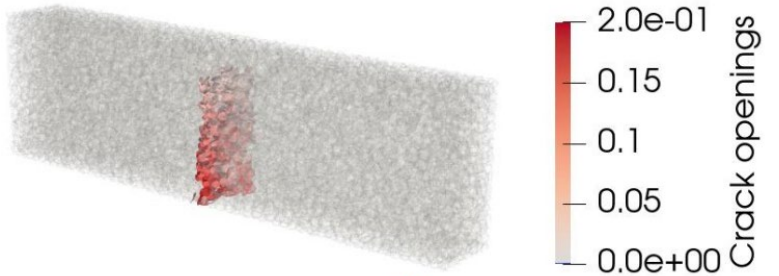

Quantitative Analysis of Model Efficiency

Julia implementation

Effect of progressive inclusion of the different numerical techniques on the computational expense, including: finite difference (FD) calculation of the Jacobian, automatic differentiation (AD), coloring-aided automatic differentiation (ColorAD), @views, StaticArray types (StArray), @inbounds, and symbolic LU factorization.

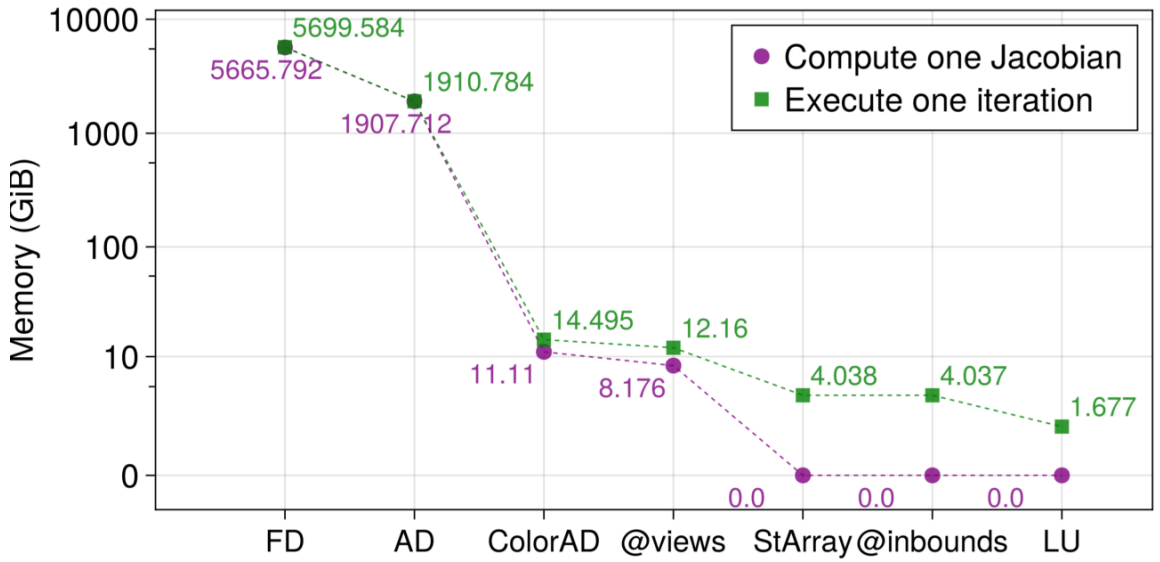

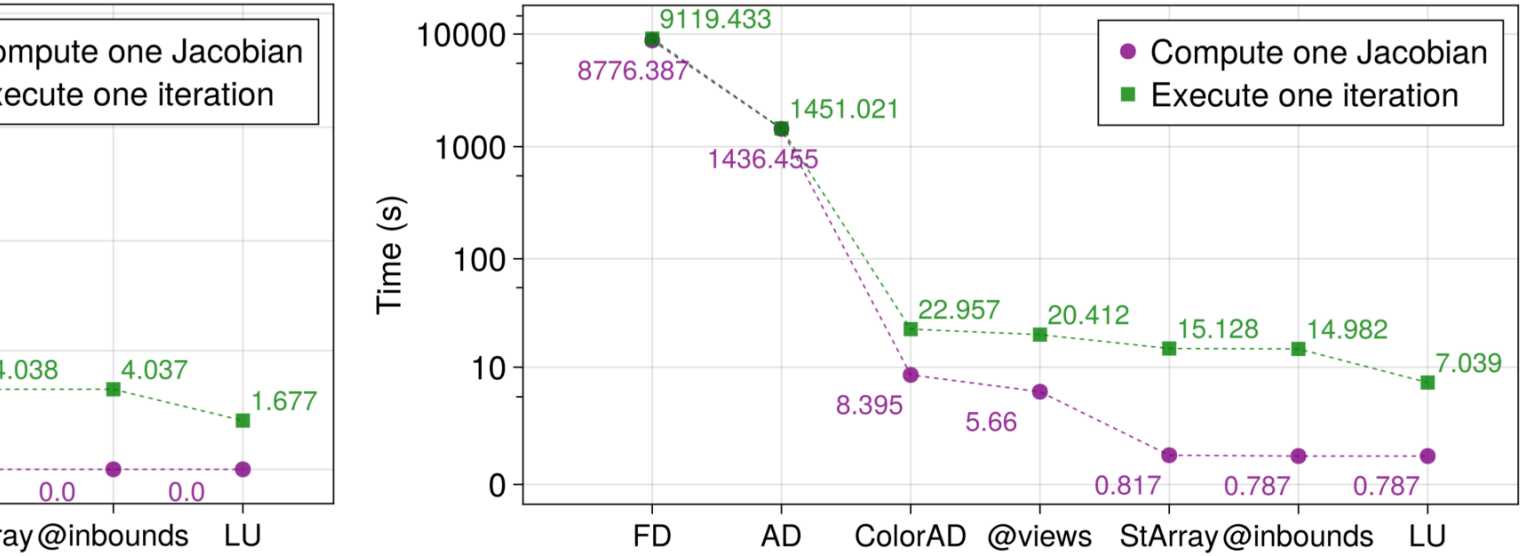

Quantitative Analysis of Model Efficiency

Improvement of computational efficiency for a three-point bending simulation

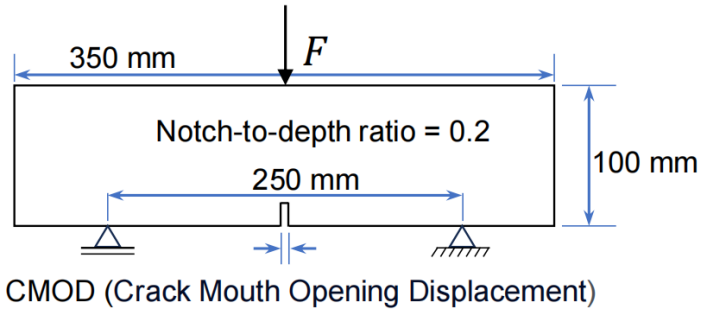

Both the memory allocation and total computational time required to reach a displacement of $0.15mm$ at the loaded point are investigated.

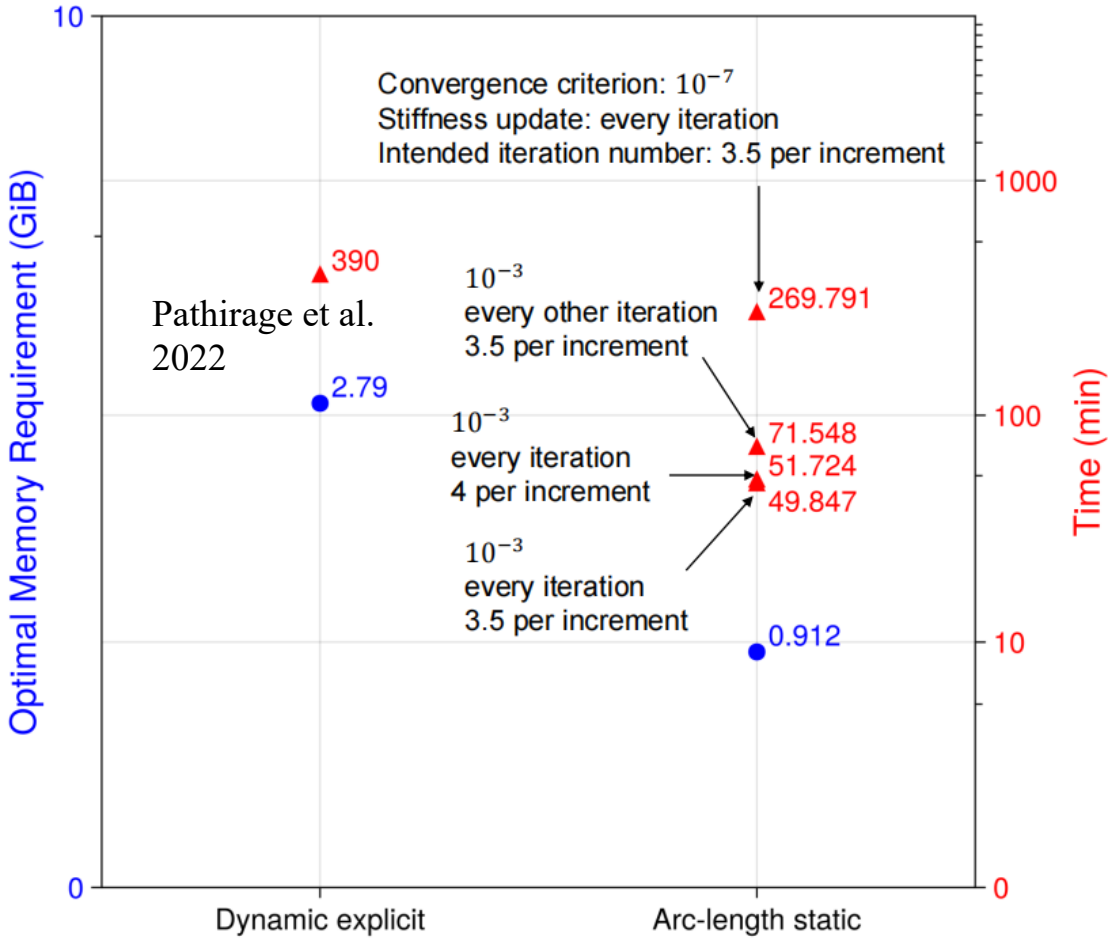

Conclusions

1. The proposed collaborative criterion to determine the sign of the initial increments of the load factor alleviates convergence issues identified with traditional arc-length methods in the solution of the LDPM governing equations.
2. Restricting path switch between the unloading-reloading and the stress limit paths at converged points is an effective way to mitigate material instabilities.
3. A smooth transition between the unloading-reloading path and the stress limit path of elements is required to obtain convergence for macroscopic stress-strain softening branches.
4. The use of automatic differentiation and graph coloring provides significant improvements in computational efficiency when evaluating the system's Jacobian matrix.
5. The proposed static solution exhibits excellent ability to capture the response curves and failure modes of concrete members under unconfined compression, biaxial loading, tensile splitting, and three-point bending.
6. The proposed implementation achieves 67% reduction in memory requirement and 87% reduction in total computational time when compared to previously available dynamic explicit solutions.

Main References

1. Jia, D., Brigham, J. C., & Fascetti, A. (2024). An efficient static solver for the lattice discrete particle model. Computer-Aided Civil and Infrastructure Engineering, under review.
2. Cusatis, G., Pelessone, D., & Mencarelli, A. (2011a). Lattice discrete particle model (LDPM) for failure behavior of concrete. I: Theory. Cement and Concrete Composites, 33(9), 881-890.
3. Cusatis, G., Mencarelli, A., Pelessone, D., & Baylot, J. (2011b). Lattice discrete particle model (LDPM) for failure behavior of concrete. II: Calibration and validation. Cement and Concrete composites, 33(9), 891-905.
4. Cusatis, G., Mencarelli, A., Pelessone, D., & Baylot, J. T. (2010). The Lattice Discrete Particle Model (LDPM) for the Simulation of Uniaxial and Multiaxial Behavior of Concrete: Recent Results. *Fracture Mechanics of Concrete and Concrete Structures-Recent Advances in Fracture Mechanics of Concrete*, 509-515.
5. Fascetti, A. (2015). *Random lattice particle modeling of fracture processes in cementitious materials* (PhD thesis). Sapienza University of Rome, Rome, Italy.
6. Pathirage, M., Thierry, F., Tong, D., Cusatis, G., Grégoire, D., & Pijaudier-Cabot, G. (2022). Comparative investigation of dynamic implicit and explicit methods for the lattice discrete particle model. In *Computational modelling of concrete and concrete structures* (pp. 503–509). CRC press.
7. Kupfer, H., Hilsdorf, H. K., & Rusch, H. (1969, August). Behavior of concrete under biaxial stresses. *In Journal proceedings* (Vol. 66, No. 8, pp. 656-666).
8. Bazant, Z. P., Kazemi, M. T., Hasegawa, T., & Mazars, J. (1991). Size effect in Brazilian split-cylinder tests. Measurements and fracture analysis. *ACI Materials Journal, 88*(3), 325-332.
9. Grégoire, D., Rojas-Solano, L. B., & Pijaudier-Cabot, G. (2013). Failure and size effect for notched and unnotched concrete beams. *International Journal for Numerical and Analytical Methods in Geomechanics, 37*(10), 1434-1452.
10. Wang, L., & Li, S. (2014). Capillary absorption of concrete after mechanical loading. *Magazine of concrete research*, 66(8), 420-431.
11. Zhang, L., Jia, J., Meng, G., & Zhu, W. (2014). Chloride diffusion in concrete subjected to compressive loading. *Magazine of concrete research, 66*(19), 991-997.

Acknowledgements

- John C. Brigham, Dongge Jia
- The Impactful Resilient Infrastructure Science and Engineering (IRISE) funding

PITT | IRISE

CENTER FOR IMPACTFUL RESILIENT INFRASTRUCTURE SCIENCE & ENGINEERING